Materials Today Bio 15 (2022) 100276

Contents lists available at ScienceDirect

Materials Today Bio

journal homepage: www.journals.elsevier.com/materials-today-bio

Programming a DNA tetrahedral nanomachine as an integrative tool for intracellular microRNA biosensing and stimulus-unlocked target regulation

Lianyu Yu [a,1], Sha Yang [a,1], Zeyu Liu [b], Xiaopei Qiu [a], Xiaoqi Tang [a], Shuang Zhao [a], Hanqing Xu [a], Mingxuan Gao [a], Jing Bao [a], Ligai Zhang [a], Dan Luo [c], Kai Chang [a,**], Ming Chen [a,d,e,*]

[a] Department of Clinical Laboratory Medicine, Southwest Hospital, Army Medical University, 30 Gaotanyan, Shapingba District, Chongqing, 400038, China
[b] Key Laboratory of Hepatobiliary and Pancreatic Surgery, Institute of Hepatobiliary Surgery, Southwest Hospital, Army Medical University, 30 Gaotanyan, Shapingba District, Chongqing, 400038, China
[c] Department of Biological and Environmental Engineering, Cornell University, Ithaca, NY, 14853, USA
[d] College of Pharmacy and Laboratory Medicine, Army Medical University, 30 Gaotanyan, Shapingba District, Chongqing, 400038, China
[e] State Key Laboratory of Trauma, Burn and Combined Injury, Army Medical University, 30 Gaotanyan, Shapingba District, Chongqing, 400038, China

ARTICLE INFO

Keywords:
DNAzyme
DNA tetrahedron
microRNA detection
Target regulation
DNA nanomaterials

ABSTRACT

The synchronous detection and regulation of microRNAs (miRNAs) are essential for the early tumor diagnosis and treatment but remains a challenge. An integrative DNA tetrahedral nanomachine was self-assembled for sensitive detection and negative feedback regulation of intracellular miRNAs. This nanomachine comprised a DNA tetrahedron nanostructure as the framework, and a miRNA inhibitor-controlled allosteric DNAzyme as the core. The DNA tetrahedron brought the DNAzyme and the substrate in spatial proximity and facilitated the cellular uptake of DNAzyme. In allosteric regulation of DNAzyme, the locked tetrahedral DNAzyme (L-tetra-D) and active tetrahedral DNAzyme (A-Tetra-D) were controlled by miRNA inhibitor. The combination of miRNA inhibitor and target could trigger the conformational change from L-tetra-D to A-Tetra-D. A-Tetra-D cleaved the substrate and released fluorescence for intracellular miRNA biosensing. The DNA tetrahedral nanomachine showed excellent sensitivity (with detection limit down to 0.77 pM), specificity (with one-base mismatch discrimination), biocompatibility and stability. Simultaneously, miRNA stimulus-unlocked inhibitor introduced by our nanomachine exhibited the synchronous regulation of target cells, of which regulatory performance has been verified by the upregulated levels of downstream genes/proteins and the increased cellular apoptosis. Our study demonstrated that the DNA tetrahedral nanomachine is a promising biosense-and-treat tool for the synchronous detection and regulation of intracellular miRNA, and is expected to be applied in the early diagnosis and tailored management of cancers.

1. Introduction

MicroRNAs (miRNAs) play a crucial part in cell proliferation, development, and maturation through the regulation at the post-transcriptional level and are therefore considered as an attractive tool to target for new therapeutic approaches [1,2]. For example, miRNA inhibitors (also called antimiRNAs) targeted at miRNA-122 have reached phase II trials for treating hepatitis [3]. On the other hand, aberrant expression of miRNAs has been attributed to many diseases including some solid tumors, myeloma and B cell lymphoma [4–6]. Consequently, miRNAs are considered as important tumor biomarkers for early cancer diagnosis and prognosis. Compared with cell-free miRNAs, intracellular miRNAs show remarkable superiority in terms of high concentration and more stability [7]. In addition, in situ detection of intracellular miRNAs, can avoid limitations in the efficiency of different RNA extraction methods [8–10]. Therefore, the establishment of highly sensitive and specific nanomachine to detect intracellular miRNAs and simultaneously regulate their concentration with negative feedback can serve as a sense-and-treat tool to improve the efficiency of early diagnosis and treatment of tumors.

* Corresponding author. Department of Clinical Laboratory Medicine, Southwest Hospital, Army Medical University, 30 Gaotanyan, Shapingba District, Chongqing, 400038, China.
** Corresponding author.
E-mail addresses: changkai0203@163.com (K. Chang), chming1971@126.com (M. Chen).
[1] Lianyu Yu and Sha Yang contributed equally to this work.

https://doi.org/10.1016/j.mtbio.2022.100276
Received 2 April 2022; Received in revised form 26 April 2022; Accepted 30 April 2022
Available online 6 May 2022

DNA is considered not only as an extraordinary carrier of genetic information but also a versatile molecular building block of nucleic acid-mediated nanostructures [11,12]. DNA self-folds into complex tertiary structures to form functional nucleic acids with specific recognition capabilities and catalytic activity such as aptamers, i-motifs, G-quadruplexes, and DNAzymes [13–15]. These functional nucleic acids show excellent potential in biomolecule detection, imaging, and drug delivery [16]. Among these functional nucleic acids, DNAzymes are single-stranded nucleic acids that can catalyze the cleavage of RNA or DNA in a metal ion-dependent manner [17,18]. Compared to protein-based enzymes, DNAzymes are much more stable, relatively easier and cheaper to synthesize, and more flexible to be programmed. In addition, DNAzymes are easily modified and functionalized, which facilitate multifunctional signal amplification and readout [19]. Based on these advantages, DNAzymes have been employed to detect metal ions [20,21], small molecules [22,23], proteins [24,25], and bacteria [26,27]. To achieve simultaneous detection and regulation of miRNAs, a miRNA inhibitor strand can be introduced to mediate activity of DNAzyme. In brief, the activity of DNAzyme depends on its conformation which is controlled by a miRNA inhibitor. The combination of miRNA inhibitor and target can trigger a conformational change from locked DNAzyme to activated DNAzyme. Importantly, the activated DNAzyme cleaves the substrate and releases fluorescence for intracellular miRNA biosensing. At the same time, our designed miRNA inhibitor competitively inhibits the interaction between miRNAs and downstream genes, resulting in regulating the functions of target cells. Thus, this miRNA inhibitor-controlled allosteric DNAzyme can be used for both miRNAs biosensing and synchronous regulation of target cells. However, the allosteric regulation of DNAzymes exhibits low cell permeability and requires suitable delivery system.

Currently, the delivery of DNAzymes and their substrates into cells mainly depends on the transfection reagents and inorganic nanomaterials [28]. However, the added components can additionally complicate DNAzyme preparation and pose undesired biocompatibility risks [29]. As a classic three-dimensional DNA nanostructure, DNA tetrahedral nanomaterials have been widely used for targeted drug delivery, photothermal therapy, and *in vivo* imaging because of their stable structure, flexible programmability, and intrinsic biocompatibility [30]. For instance, DNA tetrahedral nanomaterials have been used as nanocarriers to deliver siRNA to silence target genes or to deliver methylene blue for *in vivo* photodynamic therapy [31,32]. We believe that DNA tetrahedral nanomaterials themselves provide an alternative yet ideal route for the delivery when connected directly with other DNA functional materials including DNAzymes and substrate sequences. The advantages of using DNA tetrahedral nanomaterials are at least two folds: 1) when DNAzymes and substrate sequences are connected directly to the same tetrahedron, their physical distances are severely constrained, which will significantly increase the kinetics of random collision, resulting in a much higher catalytic activities and a much better sensitivity. 2) Our tetrahedrons are very rigid due to the fact that the sides are about 10 nm in length, well below the dsDNA's persistence length (50 nm). In addition, the tetrahedral nanostructures afford much stereo-hinderance. As a result, it is expected that our tetrahedral system strongly resist enzymatic degradation both outside and inside cells.

In this study, we developed a novel DNA tetrahedral nanomachine that serves as both a self-delivery vehicle and a biosense-and-treat tool for intracellular miRNA biosensing coupled with stimulus-unlocked target regulation (Scheme 1). Each DNA tetrahedral nanomachine is physically connected with an inhibitor-controlled allosteric DNAzyme and encapsulates it. The DNAzyme plays a dual role here: one, it carries fluorescent dyes for miRNAs biosensing and two, it delivers inhibitors for miRNAs regulation. In addition, the DNA tetrahedral nanomachine brings the DNAzyme and the substrate into a closer spatial proximity, enhancing the intracellular uptake of DNAzyme and preventing nuclease degradation. This nanomachine successfully monitors the overexpression of trace miRNAs and at the same time releases inhibitors to regulate their concentrations. The reported nanomachine provides an integrated tool for simultaneous diagnosis and treatment of diseases.

2. Results and discussions

2.1. Design principle and characterization of DNA tetrahedral nanomachine

The DNA tetrahedral nanomachine was composed of six strands (P1–P5, and the inhibitor strand I) (Fig. 1A). The three strands (P1, P2, and P4) and the partial sequences of P3 and P5 formed the main frame of the tetrahedron. In the hollow interior of the tetrahedron, the remaining 5′ end sequence of P3 was designed as a RNA-modified (rA) substrate, and the middle portion of the P5 strand was designed as an E6-type DNAzyme which is an RNA-cleaving DNAzyme [33]. To prevent the complementation of sequence 2 and sequence 2*, the P5 strand was pre-hybridized with inhibitor strand I, thus inhibiting the cleavage activity of DNAzyme. Notably, two toehold regions were designed at the 5′ and 3′ ends of inhibitor I (5′-toehold and 3′-toehold) to maintain the biostablity of this nanomachine. The 5′-toehold reacted with miRNA based on the toehold-mediated strand displacement reaction (TMSDR). Whereas the 3′-toehold was designed to inhibit the contact of active sequences (sequence 1 and sequence 4) to rA, thereby hindering the unexpected incision of binding DNAzyme to the substrate. When needed, the fluorophore (FAM) and its specific quencher (BHQ-1) were labelled on both sides of rA to monitor the DNA tetrahedral nanomachine in real

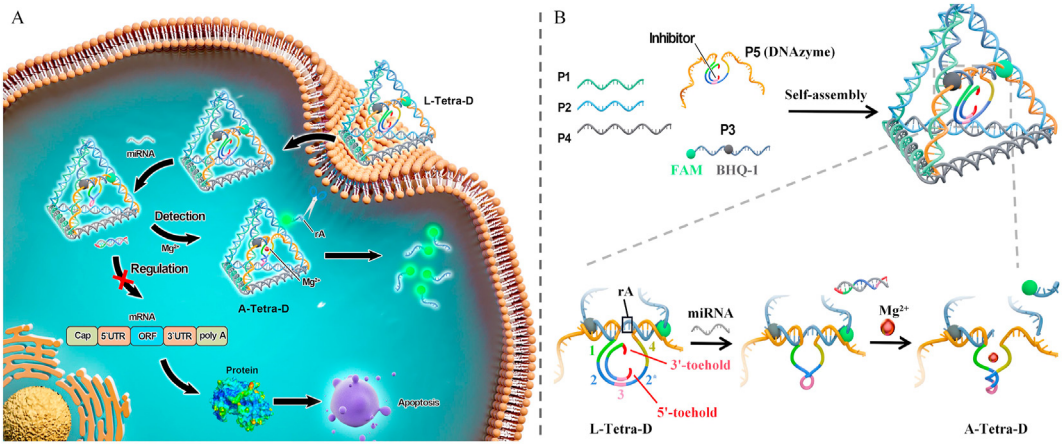

Scheme 1. (A) Schematic illustration of the mechanism of DNA tetrahedral nanomachine for specific miRNA detection and regulation in living cells. (B) DNA tetrahedral nanomachine synthesis based on internal self-assembly of six oligonucleotides and amplified reaction process.

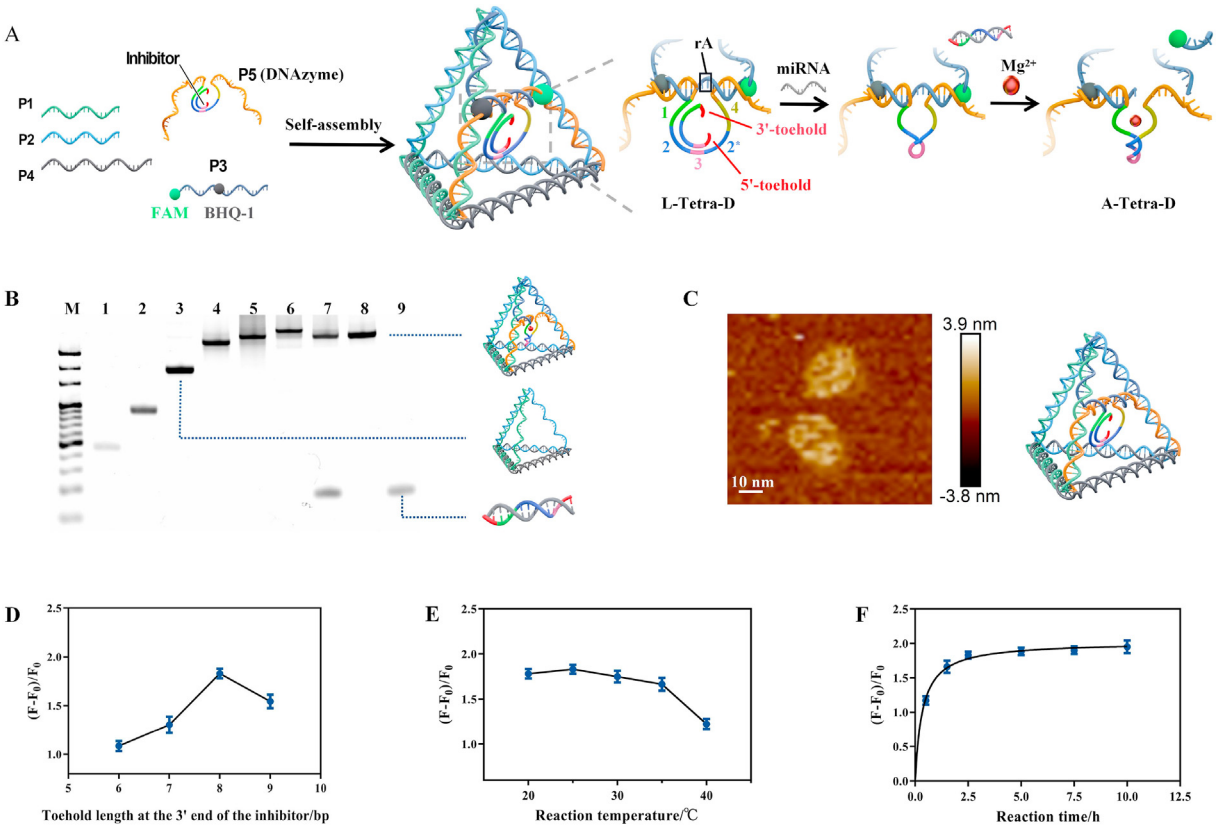

Fig. 1. Characterization and optimization of DNA tetrahedral nanomachine. (A) Experimental procedure of this DNA tetrahedral nanomachine. (B) Electrophoresis result to verify the construction of DNA tetrahedral nanomachine. Lane M: DNA ladder, Lane 1: P1, lane 2: P1+P2, lane 3: P1+P2+P4, lane4: P1+P2+P4+P5, lane 5: P1+P2+P4+P5+miRNA inhibitor strand I, lane 6: TD-DNAzyme (P1+P2+P3+P4+P5+I), lane 7: DNA tetrahedral nanomachine reacted with target miR-21,lane 8: DNA tetrahedral nanomachine without the inhibitor strand I, lane 9: the hybridization of target miR-21 and inhibitor I. (C) Characterization of DNA tetrahedral nanomachine via atomic force microscopy (AFM). Scale bars, 10 nm. (D) Optimum condition of toehold length at the 3′ end of the inhibitor. Optimum conditions of (E) reaction temperature and (F) reaction time between DNA tetrahedral nanomachine and target.

time.

The experimental procedure of this DNA tetrahedral nanomachine is shown in Fig. 1A and Fig. S1. The hairpin structure of DNA tetrahedral nanomachine (1-2-3-2*-4) was first blocked by the inhibitor strand I, forming a locked tetrahedral DNAzyme (L-tetra-D) (Fig. 1A). With addition of miRNA, miRNA can bind to 5′-toehold of inhibitor I to expose sequence 2, thus promoting the complementary binding of sequence 2 and sequence 2*, which can induce the removal of inhibitor I from L-Tetra-D based on TMSDR. Thereafter, DNA tetrahedral nanomachine restored the closed stem-loop structure from an open structure, forming an active tetrahedral DNAzyme (A-Tetra-D), which cut the substrate P3 into two pieces at the cleavage site rA. More specifically, the experimental procedure of our pure DNAzyme was further proved in Fig. S1. With addition of Mg^{2+} (lane 9), P5 could cut the Substrate into L (verified by lane 11). Whereas, in absence of Mg^{2+} (lane 12), P5 cannot cut the Substrate. So, with addition of target miRNA-21 (miR-21) in presence of Mg^{2+} (lane 8), miR-21 can bind with Inhibitor to generate Inhibitor-miR-21 duplex (verified by lane 10), and P5 can cut the Substrate into L. Moreover, based on fluorescence resonance energy transfer (FRET), the fluorescence signal was less quenched (i. e., signal enhanced) due to the increased distance between FAM and BHQ-1 (Fig. S2). On the other hand, the combination between the inhibitor strand and miRNA competitively inhibited the interaction between miRNAs and mRNAs and further regulated downstream gene/protein expression and induced tumor cell apoptosis.

The construction of the DNA tetrahedral nanomachine was verified using a 5% native polyacrylamide gel electrophoresis (PAGE) gel (Fig. 1B). As we can see from lanes 1 to 6, with the addition of new strands, the electrophoretic mobility decreased because of the increase in molecular mass and the more complex spatial structure, which suggested the successful assembly of the DNA tetrahedral nanomachine (lane 6). With addition of target miR-21 (lane 7), TMSDR was triggered, L-Tetra-D has transformed to A-Tetra-D (verified by lane 8), thus producing a hybrid product between inhibitor I and miR-21 (verified by lane 9). Although the short strand produced by the cleavage of the substrate (P3) by the DNAzyme (P5) cannot be seen in this electrophoresis gel because of its smaller molecular mass, the subsequent fluorescence experiments corresponded to the added miRNAs further validated the design of our self-assembled nanomachine (Fig. 2). The self-assembly of the DNA tetrahedral nanomachine was further verified through atomic force microscopic (AFM) images (Fig. 1C), with a diameter of 13.55 nm (Fig. S3A) with a ζ potential of ~−6.82 (Fig. S3B).

2.2. Optimizations

To achieve the best performance, several conditions that were most likely to affect the nanomachine were optimized; these conditions included the toehold length at the 3′ end of the inhibitor, the reaction temperature, and the reaction time between the DNA tetrahedral nanomachine and the target. We applied formula $(F–F_0)/F_0$, where F and F_0 were the fluorescence peak value with and without the addition of miR-21, respectively, to quantify our experiments.

We first varied the toehold lengths, from 6 to 9 bases at the 3′ end of the inhibitor, to maximize the sensitivity of the detection (Fig. 1D and Table S2). We found that the toehold length of 8 bases gave the highest change of the fluorescence signals. Notably, the toehold length at the 3′

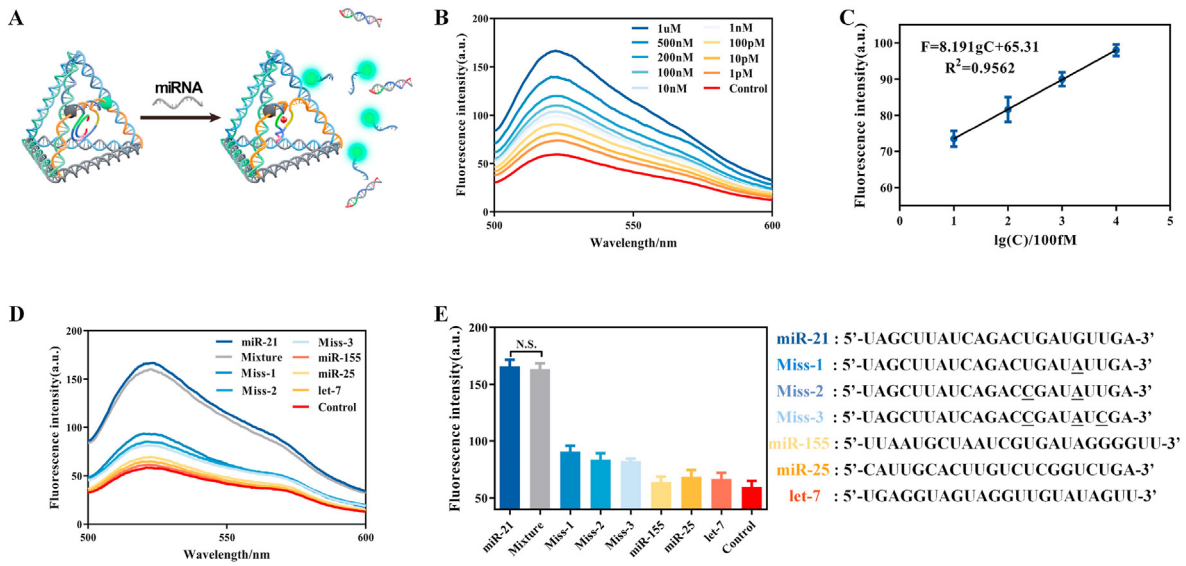

Fig. 2. Detection performance of DNA tetrahedral nanomachine *in vitro* and their feasibility *in vivo*. (A) Schematic illustration of the mechanism of DNA tetrahedral nanomachine for specific miRNA detection. (B) Fluorescence responses in the presence of different concentrations of miR-21. (C)The linear relationship between signals and miRNA concentrations. (D and E) Selectivity of DNA tetrahedral nanomachine toward Miss-1, Miss-2, Miss-3, different types of miRNAs (miR-155, miR-25, and let-7) and Mixture.

end of the inhibitor significantly affected the detection efficiency of the DNA tetrahedral nanomachine. This effect could be attributed to the dangling of the 3′-toehold, which could prolong the spatial distance between the active sequences of A-Tetra-D and rA, so as to inhibit the cutting of rA by A-Tetra-D, thereby reducing the background signal. Therefore, with toehold length increasing, the inhibiting ability of I to A-Tetra-D increased, which could decrease the background signal. But, the overlong 3′-toehold could interrupt the binding of miR-21 and 3′-toehold.

In addition, the reaction temperature also affected the performance of the nanomachine (Fig. 1E and Table S2). The maximum changes of signal were at the reaction temperature of 25 °C. With the increase of temperature, the fluorescence intensity changes decreased gradually. That's because DNAzyme has cleavage activity only when it has a hairpin structure. With reaction temperature increasing, DNAzyme tends to form a single-stranded structure, thus subsequently decreasing the cleavage activity. Thus, 25 °C was chosen as the optimal temperature for our detection.

The reaction time between DNA tetrahedral nanomachine and the target was also examined (Fig. 1F and Table S2). With increasing reaction time, the fluorescence intensity changes first increased rapidly and then gradually plateaued after 2.5 h. To achieve optimal detection efficiency in a shorter span of time and at a lower cost, the optimal reaction time for detection was determined to be 2.5 h.

Table 1
Comparison with other methods with DNAzyme.

Target miRNA	Detection Range	Lod	Intracellular Detection	Ref
miR-21	50 pM to 50 nM	16 pM	Yes	[39]
miR-21	10 pM to 1 nM	1 pM	No	[40]
miR-21	N/A	10 pM	Yes	[41]
miR-155	10 pM to 10 nM	1.6 pM	Yes	[42]
miR-141	N/A	25 pM	Yes	[43]
miR-155	0.1 nM–10 nM	44 pM	Yes	[44]
miR-141	N/A	4.6 pM	Yes	[45]
let-7b	3 pM to 10 nM	1.5 pM	No	[46]
miR-21	2 nM–300 nM	570 pM	Yes	[47]
miR-21	1 pM to 1 μM	0.77 pM	Yes	This work

2.3. *In vitro studies of the DNA tetrahedral nanomachine*

Detection was achieved when DNA tetrahedral nanomachine hybridized with miRNAs and generated stronger fluorescences (Fig. 2A). To further determine the accuracy of the nanomachine quantitatively, we monitored the corresponding changes of the fluorescence intensity with the increase of miRNA target concentrations (1 pM–1 μM) under the optimum conditions: the peak intensity at 523 nm increased gradually (Fig. 2B). The detection limit was determined to be 0.77 pM using the linear regression (1 pM–1 μM) and the rule of 3σ/slope (Fig. 2C and Table S3), which was better than other detection methods using DNAzyme (Table 1). This indicated that under the induction of the target miRNA, the structure of our DNA tetrahedral nanomachine which changed from L-tetra-D to A-tetra-D, could effectively cleave the substrates, resulting in high fluorescence signals for a very sensitive detection.

Specificity is another crucial factor, which shows that only molecules of interest can be identified. To further evaluate the specificity of the DNA tetrahedral nanomachine, single-base, double-base, and triple-base mismatched miR-21 (Miss-1, Miss-2, and Miss-3), three other homologous miRNAs (miR-155, miR-25, and let-7) and the Mixture (miR-155, miR-25, let-7 and miR-21 at the ratio of 1:1:1:1) were used as contrastive molecules (Fig. 2D and E and Table S4). In these tests of miR-21-targeted DNA tetrahedral nanomachine, the base mismatched miR-21 and the non-complementary miRNAs induced fluorescent signals that were only slightly higher than background signal. Conversely, target binding (miR-21 and Mixture) showed significant signal enhancement, indicating that the DNA tetrahedral nanomachine exhibited high specificity in distinguishing between target miRNAs and similar substances ($P < 0.05$), and was sufficient to effectively reduce false positives. However, the Mixture detection was not significantly different from the one detected for miR-21 ($P > 0.05$), suggesting that the presence of other homologous miRNAs did not disturb the biosensing of miR-21.

2.4. *Stability and biocompatibility of the DNA tetrahedral nanomachine*

When applying lots of DNA nanomachine to work inside living cells (Fig. 3A), the greatest challenges faced mainly are lack of biocompatibility and instability, since these characteristics largely determine whether these nanomachines could be transported into cells intact,

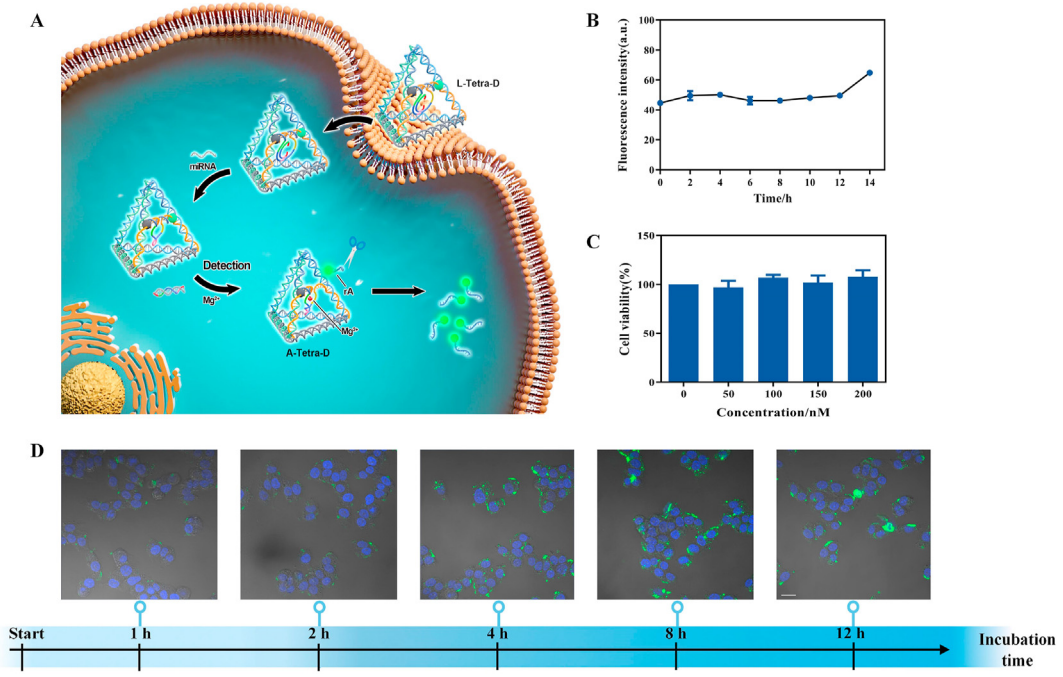

Fig. 3. (A) Schematic illustration of the mechanism of DNA tetrahedral nanomachine for intracellular miRNA detection. (B) Fluorescence characterization of DNA tetrahedral nanomachine degradation by incubating in 10% fetal bovine serum for the stated times. (C) Cell viability assay (CCK-8): HepG2 cells treated with DNA tetrahedral nanomachine of varied concentrations (0–200 nM) for 12 h at 37 °C. Error bars indicate means ± SD (n = 3). (D) Confocal fluorescence imaging of DNA tetrahedral nanomachine incubated with HepG2 cells for 1, 2, 4, 8 and 12 h. Scale bars are 20 μm.

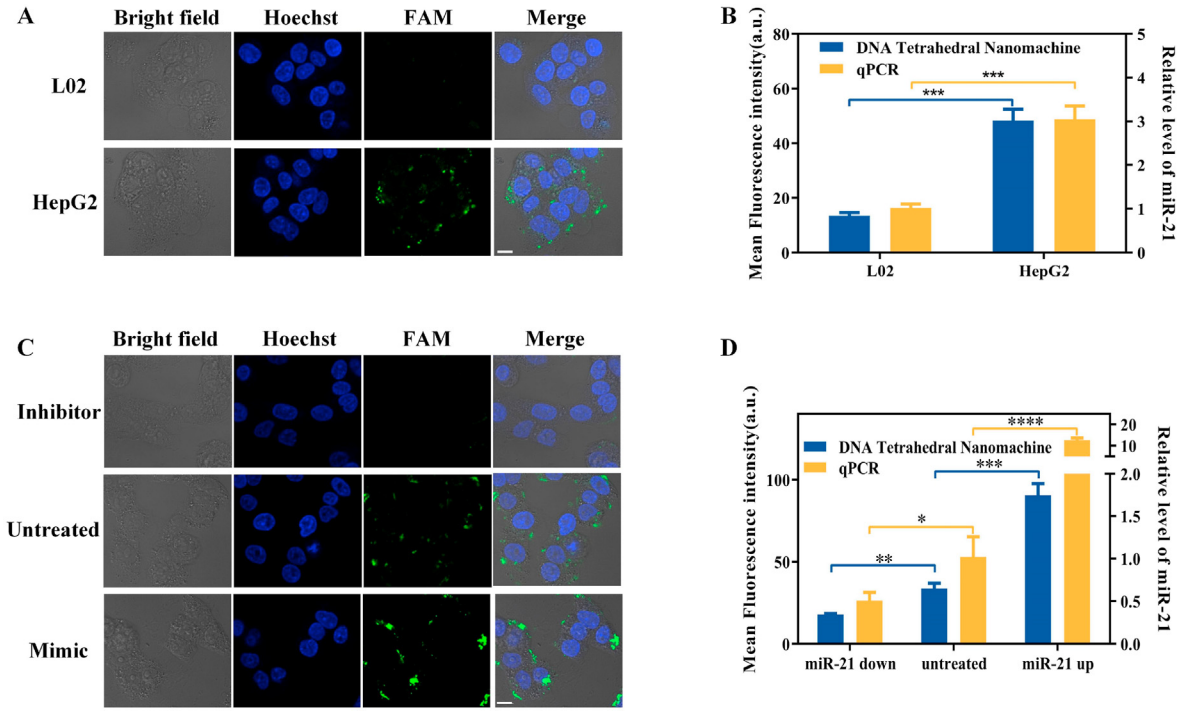

Fig. 4. Study of DNA tetrahedral nanomachine for detecting miRNAs *in vivo*. (A) Confocal fluorescence imaging of DNA tetrahedral nanomachine for detection of miR-21 in L02 cells and HepG2 cells. (B) Fluorescence intensity and the relative expression levels of miR-21 in the HepG2 cells, and L02 cells. And the relative expression levels of miR-21 in corresponding cells. (C) Confocal fluorescence imaging of DNA tetrahedral nanomachine to detect miR-21 in HepG2 cells treated with miR-21 inhibitor, untreated HepG2 cells and HepG2 cells treated with mimic. (D) Fluorescence intensity of the HepG2 cells pretreated with miR-21 inhibitor, untreated HepG2 cells and HepG2 cells treated with mimic. And the relative expression levels of miR-21 in corresponding cells. Scale bars, 10 μm. Error bars indicate means ± SD (n = 3). (*$P < 0.05$, **$P < 0.01$, ***$P < 0.001$, ****$P < 0.0001$).

function properly, and avoid false-positive signals [34,35]. To mimic physiological environment, 10% fetal bovine serum (FBS) was first used to study its stability. When incubated in 10% FBS for 0–14 h, the fluorescence intensity of DNA tetrahedral nanomachine changed negligibly, demonstrating it has a certain ability to maintain stable in complex biological samples (Fig. 3B and Table S5). Furthermore, a conventional

colorimetric CCK-8 assay was also carried out to examine the biocompatibility of DNA tetrahedral nanomachine. Different concentrations of DNA tetrahedral nanomachine were incubated with human hepatocellular cancer (HepG2) cells from 0 to 200 nM (Fig. 3C and Table S6). Low cytotoxicity or side effects were observed in living cells during the incubation with DNA tetrahedral nanomachine, and the HepG2 cells remained highly viable even when DNA tetrahedral nanomachine was used at a concentration of 200 nM. These results confirmed that the DNA tetrahedral nanomachine displayed good biocompatibility and has the potential to provide reliable results in intracellular detection and regulation.

2.5. DNA tetrahedral nanomachine-mediated intracellular miR-21 biosensing

Encouraged by the satisfactory stability and biocompatibility, the DNA tetrahedral nanomachine was further used as a powerful biosensing tool to function in live cells. HepG2 cells were chosen to examine the feasibility of the DNA tetrahedral nanomachine for *in-situ* detection of miR-21 [36,37]. Before the application of DNA tetrahedral nanomachine in living cells, its intracellular stability and the appropriate incubation times were studied. Although the previous stability test with 10% FBS could simulate the internal and external environment of the cell to a certain extent, there was still a lack of direct evidence to show the intracellular stability of the DNA tetrahedral nanomachine. Thus, in this study, HepG2 cells were incubated with DNA tetrahedral nanomachine for various times (1, 2, 4, 8 and 12 h) and the fluorescence of FAM was imaged by confocal laser scanning microscopy (Fig. 3D, Fig. S4 and Table S7). The fluorescence intensity gradually increased and stabilized at 4 h. After 8 h of incubation, the intensity continued to increase, indicating that the FRET-based quenching was relaxed and that the nanostructure was gradually disassembled, presumably by nucleases. This period of time was shorter than that observed for the DNA tetrahedral nanomachine in 10% FBS, because the intracellular condition is more complicated than FBS. These results also indicated that 4 h could be considered the optimal reaction time in the following experiments.

Subsequently, we used HepG2 cells and L02 cells (normal human liver cells) to detect the miRNA level in different cell lines (Fig. 4A). Bright green colors were observed in HepG2 cells, implying a high level of miR-21 expression. In contrast, L02 cells showed a relatively dimmer green fluorescence color compared to that in HepG2 cells, indicating a lower level of miR-21 expression. The fluorescence intensities of these two sets of images were quantified, revealing that the fluorescence intensity of HepG2 cells was 3.6 times higher than that of L02 cells which was

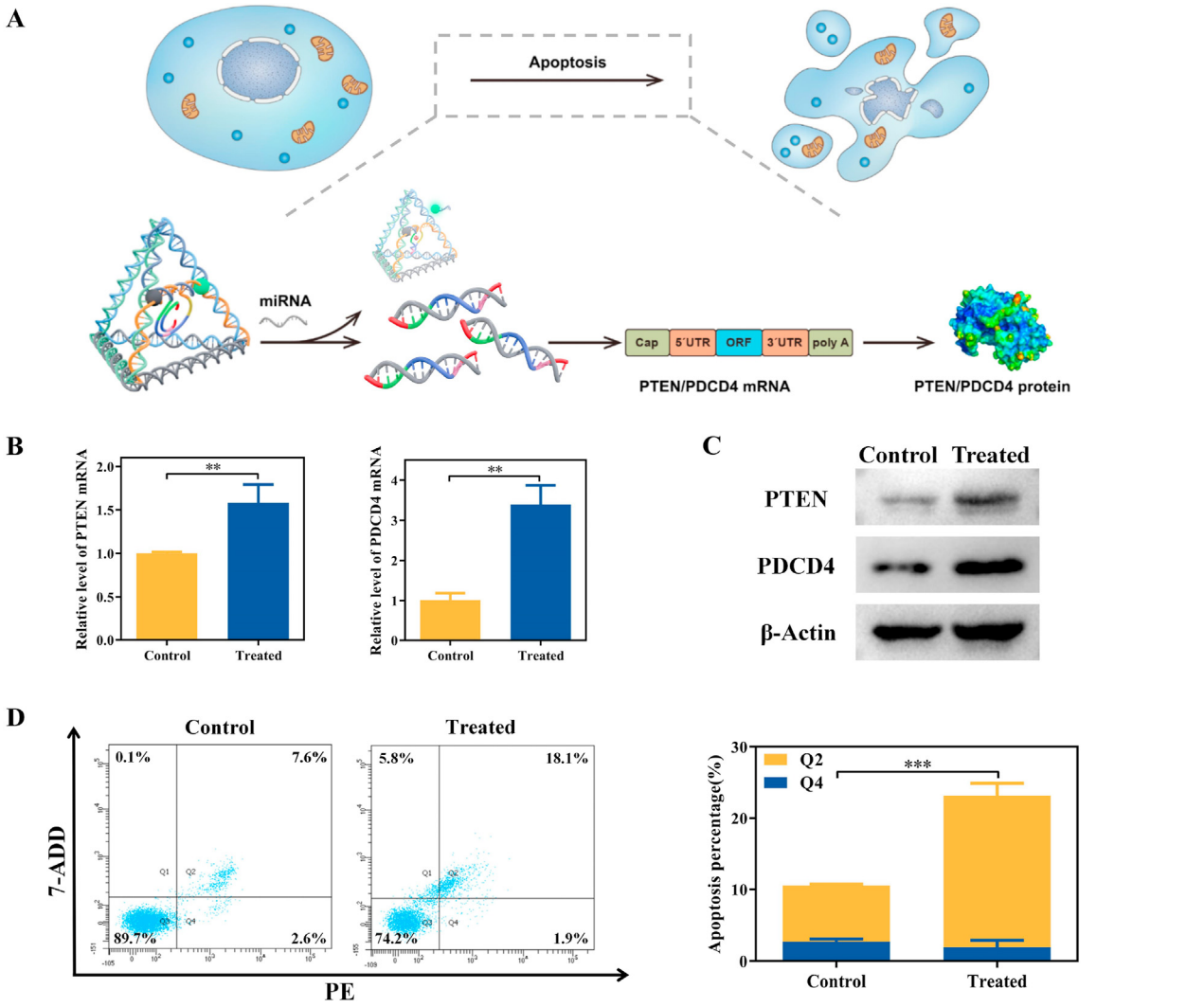

Fig. 5. Study of intracellular regulatory function of DNA tetrahedral nanomachine. (A) Schematic illustration of the mechanism of DNA tetrahedral nanomachine for synchronous cell regulation. (B) The changes of downstream mRNA expression after the regulation of DNA tetrahedral nanomachine. (C) The changes of downstream protein expression after the regulation of DNA tetrahedral nanomachine. (D) Apoptosis of HepG2 cells after incubated with 100 nM DNA tetrahedral nanomachine for 48 h. 7-AAD: 7-Amino-Actinomycin; PE: Phycoerythrin. Error bars indicate means ± SD (n = 3). (*$P < 0.05$, **$P < 0.01$, ***$P < 0.001$).

consistent with the results of gold standard quantitative reverse transcription polymerase chain reaction (RT-qPCR, Fig. 4B and Table S8). Overall, these findings indicated that DNA tetrahedral nanomachine specifically detected miRNA levels in different cells.

Since the miRNA levels vary at different stages of tumorigenesis in the same cancer cells, they can be utilized to monitor, the progress of tumor development in living cells. Towards that end, we constructed three groups of HepG2 cells with different miR-21 levels: a high miR-21 level group (pre-treated with the miR-21 mimic), a low miR-21 level group (pre-treated with the miR-21 inhibitor), and a control group without any treatment. These three groups of cells were then incubated with 100 nM DNA tetrahedral nanomachine for 4 h, and the fluorescence of FAM was evaluated (Fig. 4C). Compared with the control group, almost no fluorescence signals were detected in the low-level group. On the other hand, the high miR-21 level group showed strong green fluorescence under the same conditions, suggesting the specific stimulation of the DNA tetrahedral nanomachine. The above results also indicated that our strategy was able to semi-quantitatively detect target miRNAs in living cells. Furthermore, we verified the fluorescence intensity from images using RT-qPCR (Fig. 4D and Table S9). We obtained the similar trend, suggesting that the DNA tetrahedral nanomachine was capable of detecting miRNA levels in living cells.

2.6. Synchronous regulation of cells by the DNA tetrahedral nanomachine

After verifying the intracellular detection ability of the DNA tetrahedral nanomachine, we further investigated whether or not our nanomachine could play a regulatory role in living cells. Note that miRNAs regulate gene expressions post-transcriptionally by combining the 3′-UTR region of the corresponding mRNA. Consequently, both miRNAs and targeted genes regulate downstream effects such as the apoptosis signaling pathway. Thus, we hypothesized that the downstream mRNAs/proteins levels and/or the apoptotic events could serve as reporter signals for the regulatory function of our DNA tetrahedral nanomachine. In our design (Fig. 5A), the DNA tetrahedral nanomachine released inhibitors to recognize and hybridize with miR-21, which would lead to increase the expression of downstream PTEN/PDCD4 [38] and promoted apoptosis of HepG2 cells. Indeed, through qPCR, the expressions of PTEN and PDCD4 mRNA in DNA tetrahedral nanomachine-treated HepG2 cells, were distinctly upregulated compared to those in control HepG2 cells (Fig. 5B). Similarly, western blot demonstrated that the treated cells had a remarkably up-regulated expression of PTEN and PDCD4 protein, compared with the control cells (Fig. 5C and Fig. S5). We also measured the apoptotic events using flowcytometry to further evaluate the regulatory functions of our DNA tetrahedral nanomachine. A significantly increase in total apoptosis rate in DNA tetrahedral nanomachine-treated cells was observed (Fig. 5D). In conclusion, the upregulated levels of downstream genes and proteins as well as the increased apoptotic rate of tumor cells demonstrated the miRNA regulatory function of DNA tetrahedral nanomachine.

Table 2
Comparison with other methods for intracellular microRNA detection.

Method	Target miRNA	Detection Range	Lod	Stabilty Time	Ref
Fluorescence	miR-20a	0.45 pM–190 pM	491 fM	N/A	[48]
Fluorescence	miR-34a	1 nM–50 nM	1.499 nM	6 h	[49]
Fluorescence	miR-21	50 pM to 50 nM	16 pM	N/A	[49]
Fluorescence	miR-21	N/A	300 pM	4 h	[50]
Fluorescence	miR-146 b-5p	0.5 nM–10 nM	80 pM	5 h	[51]
Fluorescence	miR-373/ miR-96	5 nM–50 nM/ 3 nM–50 nM	590 pM/ 706 pM	4 h	[52]
Fluorescence	miR-21	10 nM to 0.5 μM	3 nM	N/A	[53]
Fluorescence	miR-141	N/A	4.6 pM	N/A	[45]
Fluorescence-SERS	miR-203	0.1 pM to 0.1 μM	630 fM	2 h	[54]
Fluorescence	miR-122	0.02 pM to 3 nM	12.5 pM	12 h	[55]
Fluorescence	miR-21	26 pM to 1 nM	26 pM	3 h	[56]
Fluorescence	miR-21	N/A	10 pM	1 h	[41]
Fluorescence	miR-21	N/A	1.3 nM	72 h	[57]
Fluorescence	miR-21	1 pM to 1 μM	0.77 pM	8 h	This work

SERS: Surface Enhanced Raman Scattering.

3. Conclusions

In our study, we developed an integrative and intelligent DNA nanomachine that could respond to intracellular miRNA targets specifically and release stimulus-unlocked inhibitors for negative feedback regulation. Owing to its unique DNA tetrahedral nanomaterials, the precisely designed DNA tetrahedral nanomachine exhibited remarkable specificity (with one-base mismatch discrimination), sensitivity (with detection limit down to 0.77 pM), biostability and self-delivery efficiency compared with other methods with DNA tetrahedron (Table S10), which are the prerequisites for the application of DNA nanomachines in living cells. By designing miRNA inhibitors as switches for regulating DNAzyme activity, our nanomachine successfully performed concurrent intracellular miRNA detection and regulation in living cells. Compared to the recently reported methods for intracellular miRNA detection (Table 2), our DNA tetrahedral nanomachine has good detection limit and stability, while maintaining well repeatability (Table S2-9). Moreover, because countless miRNAs are involved in the regulation of cellular signaling pathways, the utility of our proposed nanomachine could be extended to detect other well-studied miRNA targets and pursue gene-targeted cancer treatments by preinstalling corresponding inhibitors. As far as we know, this is the first successful attempt that DNAzyme is loaded inside a DNA tetrahedron for the simultaneous detection and regulation of miRNAs. In conclusion, this integrative nanomachine provides an integrated tool for the synchronous detection and regulation of intracellular targets and is expected to be applied in the early diagnosis and tailored management of cancers.

4. Experimental section

4.1. Materials

Oligonucleotides shorter than 60 nt were purified by high-performance liquid chromatography (HPLC) and oligonucleotides longer than 60 nt were purified by PAGE. All oligonucleotides were designed and synthesized by TaKaRa Biotechnology (China) and Sangon Biotech Co., Ltd. (China). L02 and HepG2 cells were supplied by the American Type Culture Collection (ATCC, USA). The miR-21 mimic and inhibitor were bought from RiboBio (China). The SanPrep Column MicroRNA Extraction Kit, miRNA First Strand cDNA Synthesis Kit, and 2 × SG Fast qPCR Master Mix Kit were obtained from Sangon Biotech Co., Ltd. (China). The QuantiNova Reverse Transcription Kit and QuantiNova SYBR Green PCR Kit were purchased from QIAGEN Bioinformatics (Germany). DMEM, FBS, and penicillin-streptomycin (Pen-Strep) were acquired from Biological Industries (USA). The CCK-8 kit was obtained from GenView (USA). Hoechst33342 was purchased from Invitrogen (USA). The PE Annexin V apoptosis detection kit was supplied by BD Biosciences (USA).

4.2. Instruments

The PAGE images were captured by a Bio-Rad ChemDoc XRS (Bio-Rad, USA). The fluorescence spectra were recorded using an F-7000 fluorescence spectrophotometer (Hitachi, Japan). The CCK-8 assay was performed using Thermo Scientific Variskan Flash (Thermo Fisher

Scientific, USA). The confocal imaging was conducted using a Zeiss LSM780 confocal laser scanning microscope (Zeiss, Germany). The RT-qPCR was conducted using an CFX96 Real-Time System (Bio-Rad, USA). AFM was performed by Bruker MultiMode 8 AFM (Bruker, MA, USA). Flow cytometric analysis was performed using a BD FACSCanto™ II flow cytometer (BD, USA).

4.3. Preparation of DNA tetrahedral nanomachine nanostructure

The DNA tetrahedral nanomachine consisted of 6 customized oligonucleotide chains (P1 to P5, and an inhibitor strand). The base sequences are presented in Table S1. All sequences were dissolved in a buffer (10 mM HEPES, 100 mM NaCl, and 50 mM $MgCl_2$, pH 6.0). First, DNA mixtures (P1+P2+P4, 0.02 nmol each) were denatured at 95 °C for 10 min, slowly cooled down to 20 °C and stored at 4 °C to build the tetrahedral framework. Simultaneously, for the preparation of locked-DNAzyme, the P5 and inhibitor chains were mixed in a ratio of 1:1.2, heated for 4 min at 95 °C, 30 min at 65 °C, 30 min at 50 °C, 30 min at 37 °C, 30 min at 22 °C, and maintained at 20 °C. Subsequently, P1, P2, P4, P5 and inhibitor I chains were mixed with 0.02 nmol of P3 in an equal molar ratio, heated for 10 min at 30 °C, and incubated for 1 h at 20 °C to obtain the expected DNA tetrahedral nanomachine. Moreover, the DNA tetrahedral nanomachine (20 μL) were dropped on the preconditioned dry mica substrate, the surface of which had been previously deposited with 80 μL of 1% (V/V) APTES, and after 5 min of static state, 20 μL of TE replaced residual fluids. Finally, samples were scanned using AFM.

4.4. Fluorescence measurements

For the optimization experiments, the toehold length at the 3′ end of the inhibitor, reaction temperature, and reaction time between the DNA tetrahedral nanomachine and the target were optimized to achieve high efficiency. For the sensitivity experiment, various concentrations of miR-21 from 1 pM to 1 μM was mixed with the synthetic DNA tetrahedral nanomachine. After incubation for 2.5 h at 25 °C, the fluorescence spectra were measured from 500 to 600 nm upon sample excitation at 475 nm. For the specificity tests, miR-21, different control miRNAs and Mixture were separately added into the solution containing the DNA tetrahedral nanomachine and incubated for 2.5 h at 25 °C, then the fluorescence spectra were measured. For the stability experiment, we incubated the DNA tetrahedral nanomachine with 10% FBS and recorded the FAM signal every 2 h for up to 14 h.

4.5. Cell culture and transfection of miR-21 mimic/inhibitor in HepG2 cells

L02 cells and HepG2 human hepatocellular cancer cell lines were plated in complete DMEM containing 10% FBS and 1% Pen-Strep at 37 °C in a humidified 5% CO_2. Cells (4×10^5 cells/well) were plated in 6-well plates before the transfection. On the following day, the miR-21 mimic or inhibitor with Lipofectamine 3000 were transfected into HepG2 cells for 48–72 h according to the kit's instructions. RT-qPCR was conducted to verify the results of the miR-21 mimic/inhibitor-treated cells.

4.6. Cytotoxicity test

HepG2 cells suspension (3000 cells/well) were added to 96-well plates and incubated at 37 °C overnight. Then the medium was replaced with complete DMEM containing 50 mM Mg^{2+}. Four hours later, HepG2 cells were incubated with DNA tetrahedral nanomachine of varying concentrations (0, 50, 100, 150, and 200 nM) for 12 h. Later, CCK-8 (10 μL) was added to each well and mix well. After 3 h, the optical density of the solution at 450 nm was measured to determine the cell viability.

4.7. RT-qPCR analysis of miR-21

RT-qPCR was used as a standard method to analyze the concentration of miR-21 in cells. Total cellular miRNAs were extracted using the SanPrep Column microRNA Extraction Kit in accordance with manufacturer's instructions. To detect the expression of miRNAs, the miRNA First Strand cDNA Synthesis (Stem-loop Method) Kit was used to prepare the complementary DNA (cDNA). Moreover, quantitative RT-qPCR analysis was implemented by 2 × SG Fast qPCR Master Mix Kit. Table S1 lists the primers used in the experiments. The miRNA expression results were evaluated by normalizing the expression of U6 and using the $2^{-\triangle\triangle Ct}$ method.

4.8. RT-qPCR analysis of PDCD4 and PTEN mRNAs

HepG2 cells were treated with growth medium containing DNA tetrahedral nanomachine (0.2 nmol) and Opti-MEM (180 μL) for 4 h. Then the cells were treated with fresh DMEM complete medium (2 mL) for 48 h. To detect the mRNA expression, the QuantiNova Reverse Transcription Kit was used to prepare cDNA samples, and the RT-qPCR analysis was implemented by QuantiNova SYBR Green PCR Kit. The expression results of were evaluated by normalizing the expression of β-Actin.

4.9. Western blot

HepG2 cells were treated with growth medium containing DNA tetrahedral nanomachine (0.2 nmol) and Opti-MEM (180 μL) for 4 h. Then, HepG2 cells were treated with fresh growth medium (2 mL) for 48 h. Total proteins were extracted using RIPA lysis buffer. A bicinchoninic acid assay was performed to quantify the total proteins. Then, the proteins were separated using SDS-PAGE and transferred onto NC membranes. Afterwards, the membranes were blocked with 5% fat-free milk, and the blots were probed using the corresponding antibodies overnight at 4 °C and then stained with secondary antibodies. Finally, the PTEN and PDCD4 protein bands were visualized and normalized to β-actin levels.

4.10. Confocal laser scanning microscopy (CLSM) characterization

All cell lines were plated on confocal glass dishes for 24 h in growth medium and then cultured in complete DMEM containing 50 mM Mg^{2+} for 4 h. Afterwards, the dishes were added with the DNA tetrahedral nanomachine at a final concentration of 100 nM for 4 h at 37 °C. Four percent paraformaldehyde was then used to fix the cells for 15 min. Finally, Hoechst dye was added to the confocal dishes, and the cells were treated for 10 min. All cellular fluorescence images were obtained using a laser scanning confocal microscope. L02 cells and HepG2 cells were used to determine the expression of miR-21 in different cells. The untreated HepG2 cells and miR-21 inhibitor- or mimic-treated cells were employed for the semiquantitative experiment. For the stability assay, HepG2 cells were incubated with DNA tetrahedral nanomachine for 1, 2, 4, 8, and 12 h.

4.11. Flow cytometric analysis

HepG2 cells were plated in 6-well plates (5×10^5 cells/well). On the second day, the DNA tetrahedral nanomachine (0.2 nmol) and Opti-MEM (180 μL) were added to the plates and incubated for 4 h. Then the cells were cultured in fresh complete DMEM (2 mL) for 48 h. The cells were then harvested and treated with 7-amino-actinomycin D (5 μL) and PE Annexin V (5 μL) at room temperature in the dark for 15 min. Flow cytometry was used to analyze stained cells.

4.12. Statistical analysis

All data were analyzed using SPSS 13.0 software with an unpaired,

two-tailed Student t-test. $P < 0.05$ was considered statistically significant. Each point represents the average value of three independent assays with error bars indicated.

Credit author statement

MC and KC, conceptualization and methodology, funding acquisition, project administration, writing–review & editing; LY Y and SY, resources, data curation and validation, visualization and formal analysis, writing – original draft; ZY L and XP Q, data curation and validation, visualization and formal analysis; XQ-T and SZ, software, investigation, validation; HQ X, MX G, JB and LG Z, resources, formal analysis; DL, writing–review & editing. Final approval of manuscript: All authors.

Declaration of competing interest

The authors declare that they have no known competing financial interests or personal relationships that could have appeared to influence the work reported in this paper.

Acknowledgements

This work was supported by the National Natural Science Foundation of China (Grant No. 82030066, 82122042, 81972027).

Appendix A. Supplementary data

Supplementary data to this article can be found online at https://doi.org/10.1016/j.mtbio.2022.100276.

References

[1] D. Lu, T. Thum, RNA-based diagnostic and therapeutic strategies for cardiovascular disease, Nat. Rev. Cardiol. 16 (11) (2019) 661–674.
[2] P. Khan, J.A. Siddiqui, I. Lakshmanan, A.K. Ganti, R. Salgia, M. Jain, S.K. Batra, M.W. Nasser, RNA-based therapies: a cog in the wheel of lung cancer defense, Mol. Cancer 20 (1) (2021) 54.
[3] R. Rupaimoole, F.J. Slack, MicroRNA therapeutics: towards a new era for the management of cancer and other diseases, Nat. Rev. Drug Discov. 16 (3) (2017) 203–222.
[4] S. Nucera, A. Giustacchini, F. Boccalatte, A. Calabria, C. Fanciullo, T. Plati, A. Ranghetti, J. Garcia-Manteiga, D. Cittaro, F. Benedicenti, E.R. Lechman, J.E. Dick, M. Ponzoni, F. Ciceri, E. Montini, B. Gentner, L. Naldini, miRNA-126 orchestrates an oncogenic program in B cell precursor acute lymphoblastic leukemia, Cancer Cell 29 (6) (2016) 905–921.
[5] F. Pichiorri, S.S. Suh, A. Rocci, L. De Luca, C. Taccioli, R. Santhanam, W. Zhou, D.J. Benson, C. Hofmainster, H. Alder, M. Garofalo, G. Di Leva, S. Volinia, H.J. Lin, D. Perrotti, M. Kuehl, R.I. Aqeilan, A. Palumbo, C.M. Croce, Downregulation of p53-inducible microRNAs 192, 194, and 215 impairs the p53/MDM2 autoregulatory loop in multiple myeloma development, Cancer Cell 30 (2) (2016) 349–351.
[6] M. Winkle, S.M. El-Daly, M. Fabbri, G.A. Calin, Noncoding RNA therapeutics - challenges and potential solutions, Nat. Rev. Drug Discov. 20 (8) (2021) 629–651.
[7] D. Samanta, S.B. Ebrahimi, C.A. Mirkin, Nucleic-acid structures as intracellular probes for live cells, Adv. Mater. 32 (13) (2020) 1901743.
[8] C. Chen, D.A. Ridzon, A.J. Broomer, Z. Zhou, D.H. Lee, J.T. Nguyen, M. Barbisin, N.L. Xu, V.R. Mahuvakar, M.R. Andersen, K.Q. Lao, K.J. Livak, K.J. Guegler, Real-time quantification of microRNAs by stem-loop RT-PCR, Nucleic Acids Res. 33 (20) (2005) e179.
[9] J. Koshiol, E. Wang, Y. Zhao, F. Marincola, M.T. Landi, Strengths and limitations of laboratory procedures for MicroRNA detection: table 1, Cancer Epidem Biomar 19 (4) (2010) 907–911.
[10] T.X. Lu, M.E. Rothenberg, MicroRNA, J. Allergy Clin. Immunol. 141 (4) (2018) 1202–1207.
[11] F. Li, J. Li, B. Dong, F. Wang, C. Fan, X. Zuo, DNA nanotechnology-empowered nanoscopic imaging of biomolecules, Chem. Soc. Rev. 50 (9) (2021) 5650–5667.
[12] H. Ramezani, H. Dietz, Building machines with DNA molecules, Nat. Rev. Genet. 21 (1) (2020) 5–26.
[13] Y. Tang, B. Ge, D. Sen, H.Z. Yu, Functional DNA switches: rational design and electrochemical signaling, Chem. Soc. Rev. 43 (2) (2014) 518–529.
[14] R. Micura, C. Hobartner, Fundamental studies of functional nucleic acids: aptamers, riboswitches, ribozymes and DNAzymes, Chem. Soc. Rev. 49 (20) (2020) 7331–7353.
[15] A.E. Rangel, A.A. Hariri, M. Eisenstein, H.T. Soh, Engineering aptamer switches for multifunctional stimulus-responsive nanosystems, Adv. Mater. 32 (50) (2020), e2003704.
[16] J. Kim, D. Jang, H. Park, S. Jung, D.H. Kim, W.J. Kim, Functional-DNA-driven dynamic nanoconstructs for biomolecule capture and drug delivery, Adv. Mater. 30 (45) (2018), e1707351.
[17] R.R. Breaker, G.F. Joyce, A DNA enzyme that cleaves RNA, Chem. Biol. 1 (4) (1994) 223–229.
[18] A. Ponce-Salvatierra, P. Boccaletto, J.M. Bujnicki, DNAmoreDB, a database of DNAzymes, Nucleic Acids Res. 49 (D1) (2021) D76–D81.
[19] E. McConnell, L. Cozma, Q. Mou, J. Brennan, Y. Lu, Y. Li, Biosensing with DNAzymes, Chem. Soc. Rev. 50 (16) (2021) 8954–8994.
[20] R.J. Lake, Z. Yang, J. Zhang, Y. Lu, DNAzymes as activity-based sensors for metal ions: recent applications, demonstrated advantages, current challenges, and future directions, Acc. Chem. Res. 52 (12) (2019) 3275–3286.
[21] T. Nakama, Y. Takezawa, D. Sasaki, M. Shionoya, Allosteric regulation of DNAzyme activities through intrastrand transformation induced by Cu(II)-Mediated artificial base pairing, J. Am. Chem. Soc. 142 (22) (2020) 10153–10162.
[22] H.M. Meng, X. Zhang, Y. Lv, Z. Zhao, N.N. Wang, T. Fu, H. Fan, H. Liang, L. Qiu, G. Zhu, W. Tan, DNA dendrimer: an efficient nanocarrier of functional nucleic acids for intracellular molecular sensing, ACS Nano 8 (6) (2014) 6171–6181.
[23] Y. Yang, J. Huang, X. Yang, K. Quan, H. Wang, L. Ying, N. Xie, M. Ou, K. Wang, Aptazyme-gold nanoparticle sensor for amplified molecular probing in living cells, Anal. Chem. 88 (11) (2016) 5981–5987.
[24] S. Liao, H. Ding, Y. Wu, Z. Wu, G. Shen, R. Yu, Label-free liquid crystal biosensor for L-histidine: a DNAzyme-based platform for small molecule assay, Biosens. Bioelectron. 79 (2016) 650–655.
[25] Y. Yan, C. Ma, Z. Tang, M. Chen, H. Zhao, A novel fluorescent assay based on DNAzyme-assisted detection of prostate specific antigen for signal amplification, Anal. Chim. Acta 1104 (2020) 172–179.
[26] M.M. Ali, M. Wolfe, K. Tram, J. Gu, C. Filipe, Y. Li, J.D. Brennan, A DNAzyme-based colorimetric paper sensor for Helicobacter pylori, Angew Chem. Int. Ed. Engl. 58 (29) (2019) 9907–9911.
[27] K. Tram, P. Kanda, B.J. Salena, S. Huan, Y. Li, Translating bacterial detection by DNAzymes into a litmus test, Angew Chem. Int. Ed. Engl. 53 (47) (2014) 12799–12802.
[28] J. Wei, H. Wang, Q. Wu, X. Gong, K. Ma, X. Liu, F. Wang, A smart, autocatalytic, DNAzyme biocircuit for in vivo, amplified, MicroRNA imaging, Angew. Chem. Int. Ed. 59 (15) (2020) 5965–5971.
[29] J. Wei, H. Wang, X. Gong, Q. Wang, H. Wang, Y. Zhou, F. Wang, A proteinase-free DNA replication machinery for in vitro and in vivo amplified MicroRNA imaging, Nucleic Acids Res. 48 (10) (2020), e60.
[30] C. Li, S. Luo, J. Wang, Z. Shen, Z.S. Wu, Nuclease-resistant signaling nanostructures made entirely of DNA oligonucleotides, Nanoscale 13 (15) (2021) 7034–7051.
[31] K.R. Kim, D. Bang, D.R. Ahn, Nano-formulation of a photosensitizer using a DNA tetrahedron and its potential for in vivo photodynamic therapy, Biomater Sci 4 (4) (2016) 605–609.
[32] H. Lee, A.K. Lytton-Jean, Y. Chen, K.T. Love, A.I. Park, E.D. Karagiannis, A. Sehgal, W. Querbes, C.S. Zurenko, M. Jayaraman, C.G. Peng, K. Charisse, A. Borodovsky, M. Manoharan, J.S. Donahoe, J. Truelove, M. Nahrendorf, R. Langer, D.G. Anderson, Molecularly self-assembled nucleic acid nanoparticles for targeted in vivo siRNA delivery, Nat. Nanotechnol. 7 (6) (2012) 389–393.
[33] R.R. Breaker, G.F. Joyce, A DNA enzyme with Mg(2+)-dependent RNA phosphoesterase activity, Chem. Biol. 2 (10) (1995) 655–660.
[34] R. Gao, C. Hao, L. Xu, C. Xu, H. Kuang, Spiny nanorod and upconversion nanoparticle satellite assemblies for ultrasensitive detection of messenger RNA in living cells, Anal. Chem. 90 (8) (2018) 5414–5421.
[35] A.S. Walsh, H. Yin, C.M. Erben, M.J. Wood, A.J. Turberfield, DNA cage delivery to mammalian cells, ACS Nano 5 (7) (2011) 5427–5432.
[36] R. Bose, K.S. Uday, Y. Zeng, R. Afjei, E. Robinson, K. Lau, A. Bermudez, F. Habte, S.J. Pitteri, R. Sinclair, J.K. Willmann, T.F. Massoud, S.S. Gambhir, R. Paulmurugan, Tumor cell-derived extracellular vesicle-coated nanocarriers: an efficient theranostic platform for the cancer-specific delivery of anti-miR-21 and imaging agents, ACS Nano 12 (11) (2018) 10817–10832.
[37] S. Chen, J. Zhao, C. Xu, I.Y. Sakharov, S. Zhao, Absolute quantification of MicroRNAs in a single cell with chemiluminescence detection based on rolling circle amplification on a microchip platform, Anal. Chem. 93 (26) (2021) 9218–9225.
[38] Y. Yamanaka, H. Tagawa, N. Takahashi, A. Watanabe, Y.M. Guo, K. Iwamoto, J. Yamashita, H. Saitoh, Y. Kameoka, N. Shimizu, R. Ichinohasama, K. Sawada, Aberrant overexpression of microRNAs activate AKT signaling via down-regulation of tumor suppressors in natural killer-cell lymphoma/leukemia, Blood 114 (15) (2009) 3265–3275.
[39] C. Li, C. Xue, J. Wang, M. Luo, Z. Shen, Z.S. Wu, Oriented tetrahedron-mediated protection of catalytic DNA molecular-scale detector against in vivo degradation for intracellular miRNA detection, Anal. Chem. 91 (18) (2019) 11529–11536.
[40] E. Hosseinzadeh, H. Ravan, A. Mohammadi, H. Pourghadamyari, Colorimetric detection of miRNA-21 by DNAzyme-coupled branched DNA constructs, Talanta 216 (2020) 120913.
[41] Y. Wu, J. Huang, X. Yang, Y. Yang, K. Quan, N. Xie, J. Li, C. Ma, K. Wang, Gold nanoparticle loaded split-DNAzyme probe for amplified miRNA detection in living cells, Anal. Chem. 89 (16) (2017) 8377–8383.
[42] Y. Zhang, C. Ma, C. Ma, Y. Xiang, S. Mu, Z. Zheng, X. Liu, H. Zhang, Ratiometric fluorescent detection and imaging of microRNA in living cells with manganese dioxide nanosheet-active DNAzyme, Talanta 233 (2021) 122518.
[43] Y. Yang, J. Huang, X. Yang, X. He, K. Quan, N. Xie, M. Ou, K. Wang, Gold nanoparticle based hairpin-locked-DNAzyme probe for amplified miRNA imaging in living cells, Anal. Chem. 89 (11) (2017) 5850–5856.

[44] P. Li, M. Wei, F. Zhang, J. Su, W. Wei, Y. Zhang, S. Liu, Novel fluorescence switch for MicroRNA imaging in living cells based on DNAzyme amplification strategy, ACS Appl. Mater. Interfaces 10 (50) (2018) 43405–43410.
[45] Y. Wu, J. Li, K. Quan, X. Meng, X. Yang, J. Huang, K. Wang, A DNAzyme cascade for amplified detection of intracellular miRNA, Chem. Commun. 56 (70) (2020) 10163–10166.
[46] B. Tian, Y. Han, E. Wetterskog, M. Donolato, M.F. Hansen, P. Svedlindh, M. Stromberg, MicroRNA detection through DNAzyme-mediated disintegration of magnetic nanoparticle assemblies, ACS Sens. 3 (9) (2018) 1884–1891.
[47] X. Ji, Z. Wang, S. Niu, C. Ding, DNAzyme-functionalized porous carbon nanospheres serve as a fluorescent nanoprobe for imaging detection of microRNA-21 and zinc ion in living cells, Mikrochim. Acta 187 (4) (2020) 249.
[48] Y. Fan, Y. Liu, Q. Zhoub, H. Du, X. Zhao, F. Ye, H. Zhao, Catalytic hairpin assembly indirectly covalent on FeO@C nanoparticles with signal amplification for intracellular detection of miRNA, Talanta 223 (2021) 121675.
[49] L. Zhou, M. Gao, W. Fu, Y. Wang, D. Luo, K. Chang, M. Chen, Three-dimensional DNA tweezers serve as modular DNA intelligent machines for detection and regulation of intracellular microRNA, Sci. Adv. 6 (22) (2020) b695.
[50] C. Xu, X.Y. He, X.H. Ren, S.X. Cheng, Direct detection of intracellular miRNA in living circulating tumor cells by tumor targeting nanoprobe in peripheral blood, Biosens. Bioelectron. 190 (2021) 113401.
[51] J. Gao, H. Zhang, Z. Wang, A DNA tetrahedron nanoprobe-based fluorescence resonance energy transfer sensing platform for intracellular tumor-related miRNA detection, Analyst 145 (10) (2020) 3535–3542.
[52] S. Wang, L. Zhang, A. Kan, X. Xu, N. Zhang, W. Jiang, MnO2 nanosheet-mediated target-binding-induced FRET strategy for multiplexed microRNAs detection and imaging in living cells, Talanta 226 (2021) 122202.
[53] L. Gong, S. Liu, Y. Song, S. Xie, Z. Guo, J. Xu, L. Xu, A versatile luminescent resonance energy transfer (LRET)-based ratiometric upconversion nanoprobe for intracellular miRNA biosensing, J. Mater. Chem. B 8 (27) (2020) 5952–5961.
[54] N. Zhang, S. Ye, Z. Wang, R. Li, M. Wang, A dual-signal twinkling probe for fluorescence-SERS dual spectrum imaging and detection of miRNA in single living cell via absolute value coupling of reciprocal signals, ACS Sens. 4 (4) (2019) 924–930.
[55] K. Tang, W. Wang, Z. Song, X. Luo, Multifunctional nano-biosensor based on metal-organic framework for enhanced fluorescence imaging of intracellular miRNA-122 and synergistic chemo-photothermal therapy of tumor cells, Anal. Chim. Acta 1176 (2021) 338779.
[56] M. Hu, D. Mao, X. Liu, L. Ren, M. Zhou, X. Chen, X. Zhu, An all-in-one homogeneous DNA walking nanomachine and its application for intracellular analysis of miRNA, Theranostics 9 (20) (2019) 5914–5923.
[57] X. Gao, S. Li, F. Ding, H. Fan, L. Shi, L. Zhu, J. Li, J. Feng, X. Zhu, C. Zhang, Rapid detection of exosomal MicroRNAs using virus-mimicking fusogenic vesicles, Angew Chem. Int. Ed. Engl. 58 (26) (2019) 8719–8723.